

## Synthesis, DNA Binding, DFT Calculations and Molecular Docking Studies of Biologically Active *N*-((3-(4-nitrophenyl)-1-phenyl-1*H*-pyrazol-4-yl)methylene)naphthyl Derivatives

P.V. Sandhya<sup>1</sup>, P.R. Swaran<sup>2</sup> and E. Harikrishnan<sup>3</sup>

# Asian Journal of Organic & Medicinal Chemistry

Volume: 7

Year: 2022

Issue: 2

Month: April–June

pp: 211–220

DOI: <https://doi.org/10.14233/ajomc.2022.AJOMC-P389>

Received: 12 May 2022

Accepted: 17 June 2022

Published: 29 June 2022

### ABSTRACT

Six novel pyrazole compounds were synthesized, characterized and its antimicrobial activity was also evaluated. *In vitro* antibacterial activity against diverse bacterial and fungal strains was tested and the results were compared to the standard drug. The DNA binding properties of calf thymus DNA (*ct*-DNA) were investigated using electronic absorption and fluorescence spectroscopies. The software performed computer-aided molecular docking experimentations on proteins and (*ct*-DNA). Synthesized compounds revealed moderate to satisfactory biological activities both experimentally and theoretically.

### KEYWORDS

Pyrazole derivatives, Biological activities, DNA binding, Molecular docking.

### INTRODUCTION

Heterocycles with different functionalities have recently emerged as lead compounds with different biological activities. Pyrazoles are five-membered heterocycles that are essential, significant and abundant in the structural subunits of more complex natural products such as vitamins, hormones and alkaloids [1,2]. NOS inhibitor [3], monoamine oxidase inhibitor [4], antibacterial [5], antiamebic [6], anti-inflammatory [7], antiviral, antitumor [8], antidepressant [9], anticonvulsant [10], antimicrobial, antibacterial [11], antifungal, anticancer [12], antihistaminic activities [13], proton pump inhibitor, antioxidant, antihypertensive [14], anticoagulant and agrochemical agents [15]. More, *N*-phenyl pyrazole compounds have increased biological activity, especially in antitumor and antimicrobial screening [16]. In addition, pyrazole derivatives have been found use in pesticides, herbicides and herbicides [17]. These properties make pyrazole attached derivatives an important compound in the development of new drugs.

According to the literature, compounds containing imine or azomethine groups in the skeletal have a wide range of pharmacological activities including antibacterial, antifungal, DNA and RNA inhibitory activity, protein synthesis, nitrogen fixation and carcinogenesis [18]. Imino compounds had already found application in the field of nervous system hypnotic drugs [19]. Similarly, DNA has a greater affinity for several hetero-

#### Author affiliations:

<sup>1</sup>Postgraduate and Research Department of Chemistry, Maharaja's College, Ernakulam-682016, India

<sup>2</sup>Department of Zoology, Payyanur College, Payyanur, Edat-670327, India

<sup>3</sup>Department of Botany, Payyanur College, Payyanur, Edat-670327, India

<sup>✉</sup>To whom correspondence to be addressed:

E-mail: [drsandhyapv@maharajas.ac.in](mailto:drsandhyapv@maharajas.ac.in)

Available online at: <http://ajomc.asianpubs.org>

cyclic compounds and aromatic compounds; thus, the study of the interaction between DNA and novel heterocyclic anticancer agents could have been crucial in the treatment of cancers [20]. The identification of DNA is a vital task in the antitumor action of DNA intercalators. It is noted that the intercalation is an important step in the development of several clinically utilized anticancer drugs, including anthracyclines, acridines and anthraquinones, understanding how this specific molecular interacts with DNA is essential for developing quite a selective inhibitor anticancer agent [21].

It is expected that the inclusion of a pyrazole ring in combination with an imino entity will impact the antibacterial and antifungal activities *in vitro*. A simple and reliable method is explored for generating bioactive pyrazole ended imino naphthyl compounds as part of our enduring research. Various groups on the imino naphthyl ring also were expected to influence its chemotherapeutic potential. Using IR, NMR, mass spectroscopy and elemental analysis techniques, we synthesized and characterized *N*-phenyl-*C*-phenyl ended imino naphthyl derivative products. Antimicrobial, antibacterial and antifungal exercises were also experimentally and theoretically investigated.

## EXPERIMENTAL

The Yanaco MP-S3 equipment was used to determine the melting point. A Bruker Equinox 55 FT-IR apparatus was used to record the FTIR spectra of KBr pellets. The spectra for  $^1\text{H}$  and  $^{13}\text{C}$  NMR were achieved with an NMR-JEOL GSX-400 spectrophotometer, tetramethyl silane as an internal reference and  $\text{CDCl}_3$  as a solvent. An HP 1100 LC-MS (ESI) mass spectrometer was used to obtain the mass spectra. A Cary 300 Bio (Varian) double-beam UV-Vis spectrophotometer fitted with a cuvette holder and a  $6 \times 6$  multicell Peltier frame has been used to record the electronic absorption spectra of the synthesized compounds. A Cary Eclipse spectrofluorometer was used to record fluorescence excitation and emission spectra, as well as synchronous spectra (Varian). The chemicals and reagents used here analytical grade and were not purified further.

**General procedure:** Intermediate 1-phenyl-3-nitrophenyl pyrazol-4-carboxaldehyde (**3**) was synthesized through the condensation reaction of 4-nitro acetophenone (**1**) and phenylhydrazine (**2**), preceded by the Vilsmeier-Haack reaction as shown in **Scheme-I** and then condensed with naphthyl amino deriva-

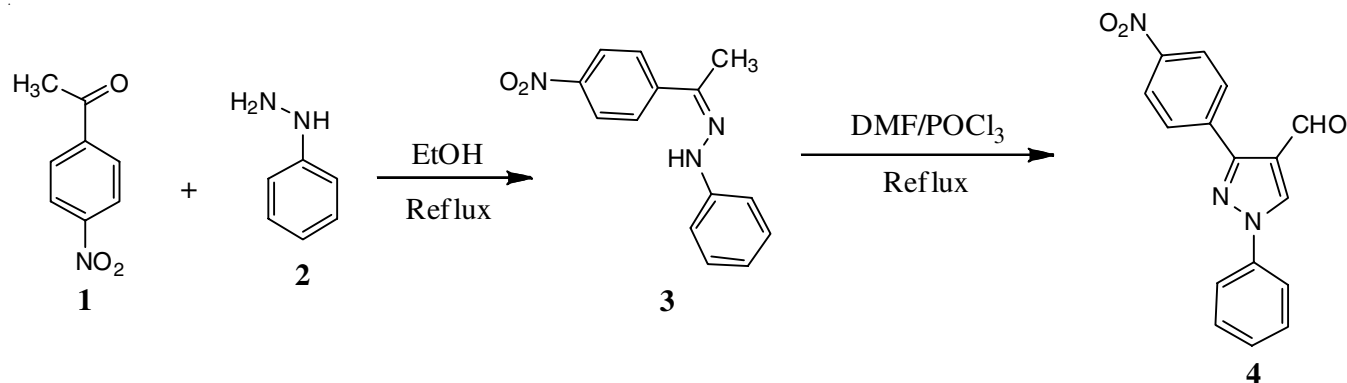
tives to yield *C*-nitro phenyl *N*-phenyl pyrazole ended imino naphthyl (**Scheme-II**).

**Synthesis of *N*-((3-(4-nitrophenyl)-1-phenyl-1*H*-pyrazol-4-yl)methylene)naphthalen-1-amine (**4a**):** When 1-phenyl-3-nitrophenyl pyrazol-4-carboxaldehyde (1 mmol) was condensed with 1-naphthylamine (1 mmol), the compound was formed. Yield: 44%, appearance, red coloured solid, m.p.:  $157^\circ\text{C}$ ,  $R_f$  (1:1 ethyl acetate:hexane) = 0.43. IR (KBr,  $\nu_{\text{max}}$ ,  $\text{cm}^{-1}$ ): 3065 (Ar-CH *str.*), 1469 (ArC=C *str.*), 1637 (C=N *str.*), 1243 (C-N *str.*),  $^1\text{H}$  NMR ( $\delta$  ppm): 10.37 (s, 1H, HC=N), 9.59 (s, 1H, CH of pyrazole ring), 7.32-8.19 (m, 15H, aromatic H),  $^{13}\text{C}$  NMR ( $\delta$  ppm): 116-153.6 (all aromatic carbons), 165.24 (HC=N, imino carbon);  $m/z$ : 420 ( $\text{M}^+$ ).

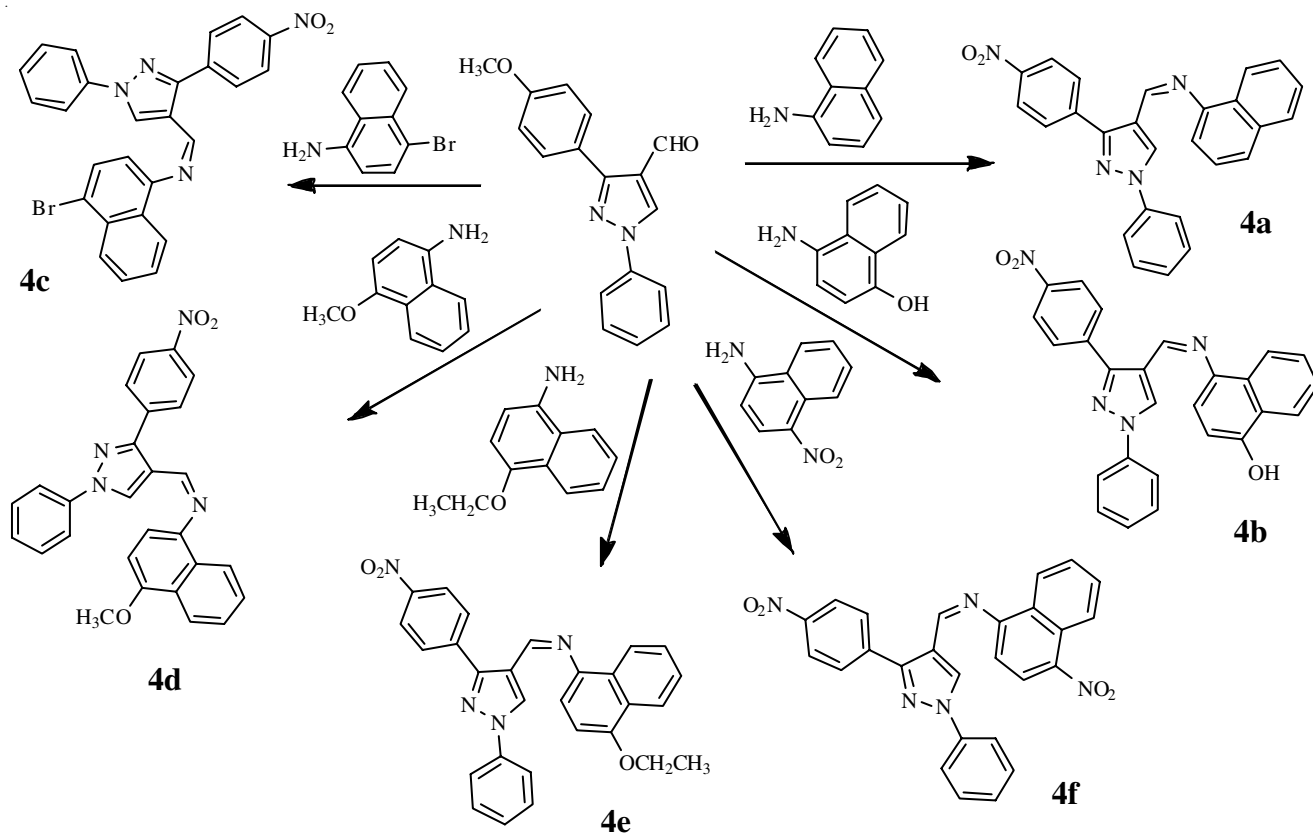
**Synthesis of 4-(((3-(4-nitrophenyl)-1-phenyl-1*H*-pyrazol-4-yl)methylene)amino)naphthalen-1-ol (**4b**):** Condensation of 1-phenyl-3-nitrophenyl pyrazol-4-carboxaldehyde (1 mmol) with 4-aminonaphthol (1 mmol) yielded compound **4b**. Yield: 33%, yellow powder, m.p.:  $128^\circ\text{C}$ ,  $R_f$  (1:1 ethyl acetate:hexane) = 0.37. IR ( $\text{cm}^{-1}$ ): 3418 (OH *str.*), 3032 (ArCH *str.*), 1457 (ArC=C *str.*), 1631 (C=N *str.*), 1235 (C-N *str.*);  $^1\text{H}$  NMR ( $\delta$  ppm): 4.96 (s, 1H, OH), 8.93 (s, 1H, HC=N), 8.44 (s, 1H, CH of pyrazole ring), 6.96-8.39 (m, 15H, aromatic H),  $^{13}\text{C}$  NMR ( $\delta$  ppm): 106-149 (all aromatic carbons), 159 (HC=N, imino carbon);  $m/z$ : 436 ( $\text{M}^+$ ).

**Synthesis of 4-bromo-*N*-((3-(4-nitrophenyl)-1-phenyl-1*H*-pyrazol-4-yl)methylene)naphthalen-1-amine (**4c**):** The compound was synthesized by reacting 1-phenyl-3-nitrophenyl pyrazol-4-carboxaldehyde (1 mmol) and 4-amino-1-bromonaphthalene (1 mmol) in a condensation reaction. Yield: 33%, dark orange powder, m.p.:  $152^\circ\text{C}$ ,  $R_f$  (1:1  $\text{CHCl}_3$ :hexane) = 0.39, (KBr,  $\nu_{\text{max}}$ ,  $\text{cm}^{-1}$ ): 3038 (ArCH *str.*), 1449 (ArC=C *str.*), 1621 (C=N *str.*), 1229 (C-N *str.*), 747 (C-Br *str.*);  $^1\text{H}$  NMR ( $\delta$  ppm): 8.99 (s, 1H, HC=N), 8.47 (s, 1H, CH of pyrazole ring), 7.05-8.52 (m, 15H, aromatic H);  $^{13}\text{C}$  NMR (ppm): 104-148 (all aromatic carbons), 169.24 (HC=N, imino carbon);  $m/z$ : 498 ( $\text{M}^+$ ).

**Synthesis of 4-methoxy-*N*-((3-(4-nitrophenyl)-1-phenyl-1*H*-pyrazol-4-yl)methylene)naphthalen-1-amine (**4d**):** To obtain compound **4d**, a condensation reaction was performed between 1-phenyl-3-nitrophenyl pyrazol-4-carboxaldehyde (1 mmol) and 4-amino-1-methoxynaphthalene (1 mmol). Yield: 32%, dark yellow solid, m.p.:  $125^\circ\text{C}$ ;  $R_f$  (1:1  $\text{CHCl}_3$ :hexane) = 0.46, (KBr,  $\nu_{\text{max}}$ ,  $\text{cm}^{-1}$ ): 3031 (ArCH *str.*), 1449 (ArC=C *str.*), 1609 (C=N *str.*), 1223 (C-N *str.*);  $^1\text{H}$  NMR ( $\delta$  ppm): 3.12 (s, 3H,



**Scheme-I:** Schematic representation of synthesis of 3-(4-nitro phenyl)-1-phenyl-1*H*-pyrazole-4-carboxaldehyde



OCH<sub>3</sub>), 9.19 (s, 1H, HC=N), 8.53 (s, 1H, CH of pyrazole ring), 7.072-8.29 (m, 15H, aromatic H), <sup>13</sup>C NMR (ppm): 105-148 (all aromatic carbons), 163.82 (HC=N, imino carbon), 52 ppm (methoxy carbon); *m/z*: 450 (M<sup>+</sup>).

**Synthesis of 4-ethoxy-*N*-((3-(4-nitrophenyl)-1-phenyl-1*H*-pyrazol-4-yl)methylene)naphthalen-1-amine (4e):** This was synthesized by the condensation reaction of 1-phenyl-3-nitrophenyl pyrazol-4-carboxaldehyde (1 mmol) and 4-amino-1-ethoxy naphthalene (1 mmol, e). Yield: 31%, dark yellow solid, m.p.: 138 °C, *R<sub>f</sub>* (1:1 CHCl<sub>3</sub>:hexane) = 0.35, (KBr, *v*<sub>max</sub>, cm<sup>-1</sup>): 3047 (ArCH *str.*), 1468 (ArC=C *str.*), 1629 (C=N *str.*), 1232 (C-N *str.*); <sup>1</sup>H NMR (ppm): 1.13 (t, 3H, CH<sub>3</sub>), 4.58 (q, CH<sub>2</sub>), 9.14 (s, 1H, HC=N), 8.42 (s, 1H, CH of pyrazole ring), 7.01-8.29 (m, 15H, aromatic H), <sup>13</sup>C NMR (ppm): 104-141 (all aromatic carbons), 165.3 (HC=N, imino carbon), 52 and 74 ppm (ethoxy carbon); *m/z*: 465 (M<sup>+</sup>).

**Synthesis of 4-nitro-*N*-((3-(4-nitrophenyl)-1-phenyl-1*H*-pyrazol-4-yl)methylene)naphthalen-1-amine (4f):** The compound was synthesized by combining 1-phenyl-3-nitrophenyl pyrazol-4-carboxaldehyde (1 mmol) and 4-nitro-naphthylamine (1 mmol). Yield: 38%, reddish brown solid, m.p.: 142 °C; *R<sub>f</sub>* (1:1 CHCl<sub>3</sub>:hexane) = 0.45, (KBr, *v*<sub>max</sub>, cm<sup>-1</sup>): 3048 (ArCH *str.*), 1452 (ArC=C *str.*), 1619 (C=N *str.*), 1219 (C-N *str.*), 1399 and 1544 (NO<sub>2</sub> *str.*); <sup>1</sup>H NMR (δ ppm): 10.37 (s, 1H, HC=N), 9.62 (s, 1H, CH of pyrazole ring), 7.39-8.26 (s, 1H, CH of pyrazole ring), 7.39 (m, 15H, aromatic H), <sup>13</sup>C NMR ppm range: 104-148 (all aromatic carbons), 168.3 (HC=N, imino carbon). *m/z*: 464 (M<sup>+</sup>).

**Antibacterial activities:** All the synthesized imino naphthyl pyrazole compounds were tested for antibacterial activity using

common procedures from the literature [22]. Ciprofloxacin was tested *in vitro* against a representative panel of bacteria, which include *Escherichia coli* MTCC 443, *Pseudomonas aeruginosa* MTCC-1688, *Staphylococcus aureus* MTCC-96 and *Streptococcus pyogenes* MTCC-442, acting as the standard drug here.

**Antifungal activity:** To study the antifungal activity, two fungal strains, *Candida albicans* MTCC-227 and *Aspergillus niger* MTCC-28, fluconazole were chosen as the standard antifungal drug. The broth microdilution method calculates the minimal inhibitory concentration (MIC) in accordance with National Committee for Clinical Laboratory Standards (NCCLS) [23].

**Antitubercular activity:** The antitubercular activity of *M. tuberculosis* H37Rv *in vitro* was investigated using a microplate Alamar blue assay (MABA) [24]. All the synthesized compounds might have fragile antitubercular activity at MIC 12.8 μg/mL, compared to 0.4 μg/mL for the standard drug INH, which could be contributed to their lower lipophilicity and thus lowered cell wall permeation.

**Molecular docking:** Molecular docking has been used to investigate the compounds' interrelations with the target protein, DNA or both and to detect the possible modes of action participating in the inhibition process. Following molecular docking with protein using the software Arguslab 4.0.1 version, the binding conformations of the prepared compound and its free energy of binding within the active site of protein thymidylate kinase (TMPK) (PDB Id: 4QGG downloaded from the PDB database) were listed. All water molecules, miscellaneous residues and heterocyclic moieties were excluded from

the protein's crystallographic structure before docking and hydrogen atoms were added to the protein's amino acid residues to stimulate the binding site only for the synthesized compound. For docking, a calculation box with  $60 \times 60 \times 60$  grid cells in XYZ directions was constructed and located in the middle of the binding site residues. The docking procedure was carried out under the supposition that the protein is rigid, the ligand molecule is flexible (all rotatable bonds of ligands are considered) and the analyses were carried out with standard precision and default values.

**UV-Vis absorption:** Determinations of UV-vis absorption spectrum were performed at pH 7.6 in 0.01 M tris buffer. Sigma-Aldrich provided and used calf thymus DNA (ct-DNA) (Saint Louis, USA). The DNA concentrations were determined using the molar extinction coefficient  $6600 \text{ M}^{-1} \text{ cm}^{-1}$  at 260 nm after sonicating the ct-DNA solution in tris buffer for 5 min [25,26]. The concentration of DNA was measured using micro-molar equivalents of base pairs and its purity was calculated by measuring the A 260/A 280 ratio. Imino naphthyl pyrazole derivatives were dissolved in DMSO at a concentration of 1 mM (stock solution) and working solutions with concentration ranging from 10 to 50  $\mu\text{M}$  were prepared by dilution with tris buffer. After optimizing the compound concentration, ct-DNA titration with constant pyrazole derivative concentrations was performed. At 25 °C, all the measurements were taken in a rectangular quartz cuvette with a 1 cm path length. The intrinsic binding constant ( $K_b$ ) was calculated by fitting the data to eqn. 1 [26]:

$$\frac{[\text{DNA}]}{(\epsilon_a - \epsilon_f)} = \frac{[\text{DNA}]}{(\epsilon_b - \epsilon_f)} + \frac{1}{K_b(\epsilon_b - \epsilon_f)} \quad (1)$$

where  $\epsilon_a$ ,  $\epsilon_b$  and  $\epsilon_f$  are the apparent, bound with DNA and free extinction coefficients of compounds, respectively.  $\epsilon_a$ ,  $\epsilon_b$  and  $\epsilon_f$  are all calculated from the Beer-Lambert's law ( $\epsilon = A/[\text{compound}]$ ). Plot fitting of  $[\text{DNA}]/(\epsilon_a - \epsilon_f)$  vs.  $[\text{DNA}]$  used and  $K_b$  acquired from the ratio of the slope to the y-intercept. The binding data were contoured using the Origin 8.0 software (OriginLab Corporation, Northampton, USA).

**Measurements of fluorescence:** Fluorescence studies on non-bound derivatives were carried out with a solution concentration of 15  $\mu\text{M}$  in 0.01 M tris buffer, pH 7.6. A rectangular quartz cuvette with a 1 cm path length and a temperature of 25 °C was used to scan emission spectra in the 380-600 nm range with an excitation wavelength of 356-364 nm. Fluorescence intensities were expressed in arbitrary units. Fluorescence titrations were performed by injecting increasing amounts

of ct-DNA (0-120  $\mu\text{M}$  bp) directly into the cell containing derivative solutions. Using the following equation, the Stern-Volmer constant ( $K_{SV}$ ) was calculated using the fluorescence intensities of compound solutions revealed to different ct-DNA concentrations (eqn. 2) [27]

$$\frac{F_0}{F} = 1 + K_{SV}[Q] \quad (2)$$

where  $[Q]$  denotes the quencher concentration,  $F_0$  and  $F$  denote the steady-state fluorescence intensities of compounds in the absence and presence of quencher (ct-DNA) and  $K_{SV}$  denotes the Stern-Volmer quenching constant.

## RESULTS AND DISCUSSION

The synthetic route for *N*-phenyl-*C*-nitrophenyl pyrazole terminated imino naphthyl derivatives is shown in **Scheme-II**. By condensing 4-nitroacetophenone with phenyl hydrazine, accompanied by the Vilsmeier-Haack reaction, the intermediate substituted pyrazole-4-carboxaldehyde was successfully synthesized. Condensing *C*-nitrophenyl *N*-phenyl pyrazol-4-carboxaldehyde with substituted naphthyl amines yielded pyrazole terminated imino naphthyl derivatives that were all well-characterized using various spectroscopic techniques.

**Antibacterial activity:** Among the pyrazole terminated imino naphthyl derivatives, **4c** and **4f** have greater antibacterial activity against *S. aureus* than **4a** and **4e**. Compounds **4b**, **4c** and **4d** are all active against *E. coli*, whereas compounds **4a** and **4e** are not. *P. aeruginosa* has a higher affinity for **4c** and **4f** and a lower affinity for **4e**. *S. pyrogenes* exhibited activity against **4b**, **4c** and **4f**, but only minor activity against **4a** and **4e**. Furthermore, with MICs of 0.2  $\mu\text{g/mL}$  against *A. niger*, these derivatives outperformed fluconazole in antifungal activity and this activity was found to be independent of the substituents. All showed good activity against *C. albicans* (MIC 50  $\mu\text{g/mL}$ ) when compared to standard fluconazole (MIC 30  $\mu\text{g/mL}$ ) (Table-1).

**Relationship between structure and activity (SAR):** The pharmacological potentiality of delocalized conjugated compounds is enhanced by an electron-withdrawing or electron-donating moiety attached to the aryl ring. Furthermore, the bioactivity of these compounds could be attributed to a combination of factors, including the number of phenyl groups attached to the pyrazole ring, the substituent on the phenyl group, the presence of imino linkage, steric hindrance, the extent of conjugation and the presence of aryl rings on the

TABLE-1  
ANTIBACTERIAL, ANTIFUNGAL AND ANTITUBERCULOSIS ACTIVITIES OF  
PYRAZOLE CLUBBED PHENYL DERIVATIVES (INHIBITION ZONE MEASURED IN mm)

Compound	<i>S. aureus</i>	<i>E. coli</i>	<i>P. aerugi</i>	<i>S. pyrogenes</i>	<i>A. niger</i>	<i>C. albicans</i>	<i>M. tuberculosis</i>
<b>4a</b>	16	15	17	14	0.2	100	100
<b>4b</b>	13	15	21	17	0.2	75	100
<b>4c</b>	20	21	21	21	0.2	100	30.2
<b>4d</b>	14	18	17	18	0.2	100	30.2
<b>4e</b>	19	17	17	16	0.2	100	100
<b>4f</b>	23	20	22	21	0.2	50	30.2
Ciprofloxacin	24	22	23	23	–	–	–
Fluconazole	–	–	–	–	30	30	–
INH	–	–	–	–	–	–	0.4

Highly active-20-30, moderately active-15-20, weakly active -11-15, less than 11 inactive

imino linkage. In most cases, any benzene ring substituent, whether electron-withdrawing or electron-donating, increased activity against all of the tested bacterial strains. Furthermore, the presence of an electron-withdrawing group on the benzene ring outperformed the presence of an electron-donating group. SAR experiments were conducted to predict the effect of various substituted imino naphthyl rings on biological activity and their electronic effect on microbial strains [24]. To create a different electronic environment around the new molecules, the naphthyl ring attached to the imino entity was substituted with electron-donating and withdrawing groups. Electron-donating substituents in the aromatic system were methoxy and ethoxy, while electron-drawing groups were hydroxy, nitro and bromo [25].

Compounds with electron-withdrawing groups (on the imino naphthyl ring) have a high level of biological activity, according to the present findings. Furthermore, the presence of hydrophobic groups at the naphthyl moiety's fourth position improves antimicrobial activity and physico-chemical properties. The activity order is  $\text{NO}_2 > \text{Br} > \text{OH} > \text{H} > \text{OCH}_3 > \text{OCH}_2\text{CH}_3$  (substituent at the 4<sup>th</sup> position of imino naphthyl ring) [26-28]. Besides that, chain length is inversely proportional to pharmacological efficacy and in our study, the methoxy compound was significantly more active than the corresponding ethoxy compounds [29]. Compounds with electron-withdrawing groups on the naphthyl ring, such as bromo, nitro and hydroxy, outshone electron-donating substituted methoxy and ethoxy derivatives against *E. coli*. Similarly, electron-withdrawing groups at the fourth position of imino naphthyl ring demonstrated activity against *S. aureus* (MIC= 12.5  $\mu\text{g}/\text{mL}$ ). At 50  $\mu\text{g}/\text{mL}$  MIC, derivatives of nitro, bromo and hydroxy substituents at the fourth position of imino naphthyl groups exceed *S. pyogenes* (Table-1).

**Protein molecular docking experiments:** Antibacterial drugs typically work by inhibiting cell wall synthesis, protein synthesis, nucleic acid synthesis or anti-metabolism [24]. In other words, it interacts with the specific proteins responsible for the routes. Thymidylate kinase (TMPK) was chosen as the target protein for molecular docking because it contains 50 monophosphate kinase and is the essential enzyme that catalyzes the biosynthesis of bacterial cell wall DNA, generating dTTP [30]. It interacts with the specific proteins responsible for the routes. Ciprofloxacin, a common antibiotic, inhibits cell wall synthesis by inhibiting the DNA gyrase enzyme required for bacterial DNA splitting. Table-2 shows the results of docking compounds **4a-f** in the binding centre of the target protein TMPK using the web application Arguslab 4.0.1 (Fig. 1). The length of the H bonds close to the active sites of the proteins was also measured. The active docking site was created using

Autodock, which forced the ligands to bind within the active site of the protein TMPK.

**Binding energy:** Estimating the ligand's binding free energy within the protein's active site is used to interpret the precision of binding affinity between the target protein and the docking models. The lower the value of binding energy, the stronger the ligand's binding within the protein. Furthermore, the ligand-protein docked compounds were examined to calculate the binding strength; the ligand interaction pattern (hydrogen/hydrophobic) and H-bond length were calculated from these minimum binding energy values. The synthesized compounds had good binding energy values ranging from -10.21 to -11.23 Kcal/mol, as shown in Table-2. According to the literature, the compounds would fit well if the predicted binding energy values were less than 2.5 Kcal/mol. According to the literature, compounds would fit well in the active pocket of the targeted protein if the predicted binding energy values were less than 2.5 Kcal/mol and all the synthesized compounds have a low binding energy and thus fit well in the active site of TMPK.

**Binding pocket and structure-activity relationship analysis:** Docking studies revealed how well the ligand bonded within the active site of the target protein as shown in Fig. 2. Compound **4f** was chosen to investigate its binding profile within the active site of the target protein. The docking study aided in understanding how the compound **4f** strongly binds within the binding pocket of TMPK, impeding TMPK's action for DNA synthesis. The amino acid residues 267 ALA, 269 LEU, 319 LEU and the ligand **4f** interact electrostatically. 270 PHE, 271 ALA, 265 THR, 268 MET, 115 LEU, 64 MET, 322 PHE, 60 ARG, 107 ILE and 112 VAL are some other amino acids that bind with compound **4f** via pi-sigma bonding. With bond distances of 1.902 and 1.749 Å, respectively, there are two H-bond interactions, one with amino acid 269 LEU and the other with N of the naphthyl ring's  $\text{NO}_2$  moiety. The structure of the synthesized compounds, according to molecular docking studies, could be used as a therapeutic agent for bacterial infections. The amino acid moiety 268 MET, 269 LEU, 265 THR, 267 ALA and 266 GLU forms five H-bonds with the compound **4b**, with bond lengths of 2.22, 1.70, 1.428, 2.96 and 2.48 Å, respectively. With the O of  $\text{CH}_3$ , the compound **4d** forms one H bond with 269 LEU and a bond length of 1.77 Å. Similarly, compounds **4e** showed two distinct H bonds with 269 LEU and 268 MET, with bond lengths of 1.555 and 1.89 Å, respectively. Compounds **4a** and **4c** do not interact with H bonds.

**DNA binding research:** The absorption spectra of the various pyrazole terminated imino naphthyl derivatives **4a-f**

TABLE-2  
BINDING ENERGY OF THE COMPOUND AND H-BOND LENGTH CALCULATED USING ARGUS LAB 4.0.1

Compound	Binding energy (Kcal/mol)	H bond length (Å)
<b>4a</b>	-11.23	-
<b>4b</b>	-11.09	2.22 (268 MET with OH), 1.70 (269 LEU with OH), 1.428 (265 THR with OH), 2.96 (267 ALA with OH), 2.48 (266 GLU with OH)
<b>4c</b>	-10.87	-
<b>4d</b>	-10.77	1.77 (269 LEU with $\text{OCH}_3$ )
<b>4e</b>	-10.92	1.555 (269 LEU with $\text{OCH}_2\text{CH}_3$ ), 1.89 (268 MET with $\text{OCH}_2\text{CH}_3$ )
<b>4f</b>	-10.21	1.902 (269 LEU with naphthyl $\text{NO}_2$ ), 1.749 (268 MET with naphthyl $\text{NO}_2$ )

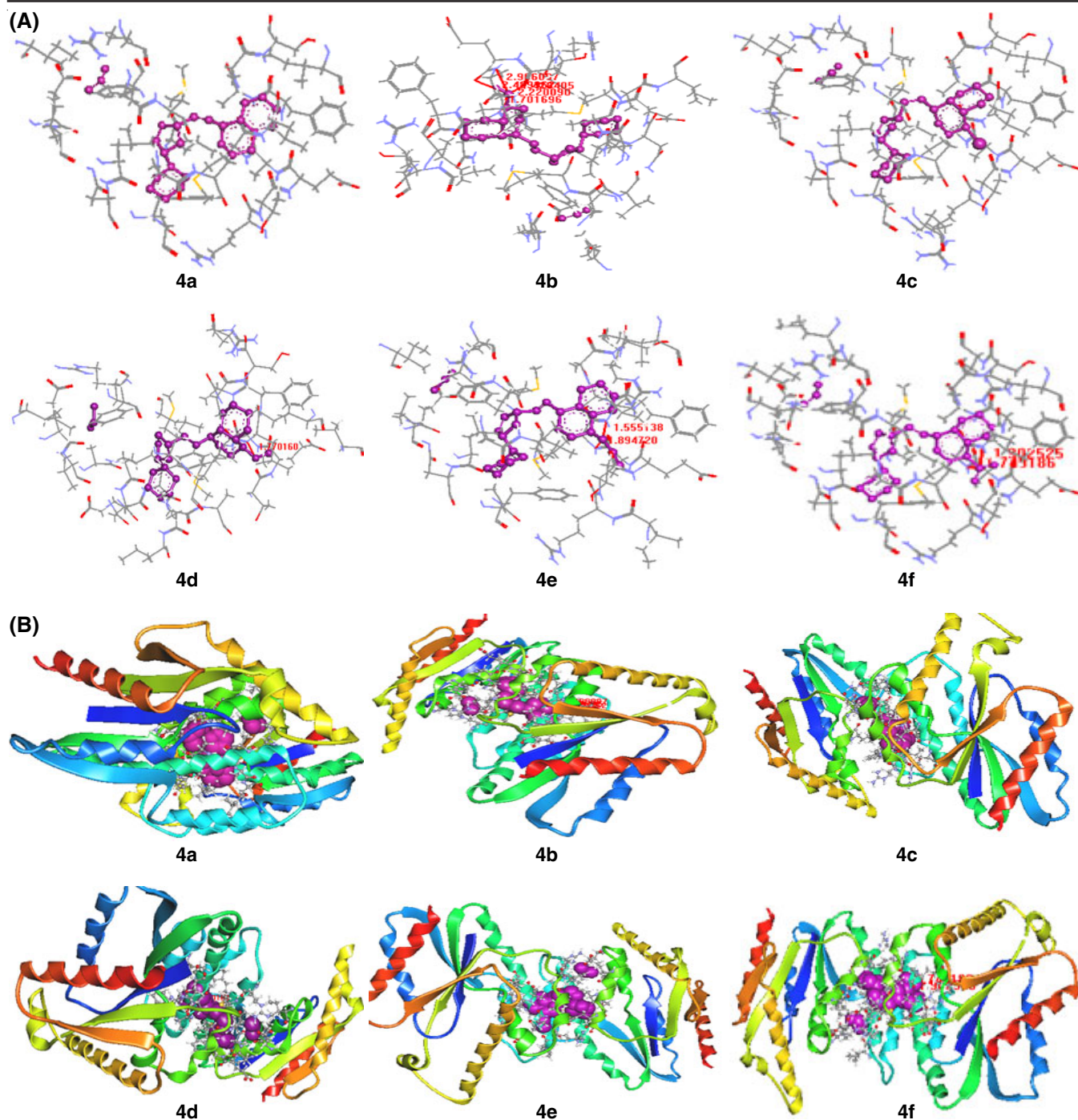


Fig. 1. Docked pose of the compounds (**4a-f**, purple) in the active site of the target protein (grey and blue colour (A) and its cartoon view (protein as ribbon) (B)

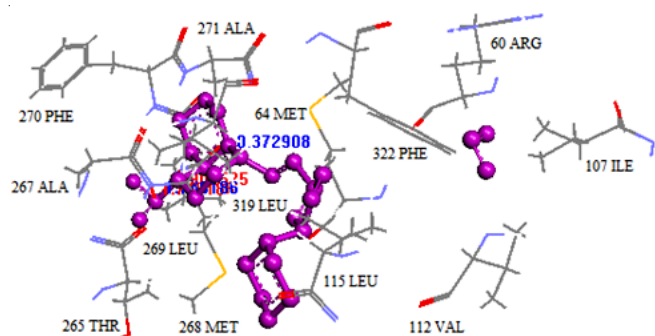


Fig. 2. Closer view of docking complex to justify the interaction behaviour of **4f** against the target protein

show that they all have absorption bands in the 300-500 nm range. Except for compound **4f**, the different donor or acceptor substituents in compounds **4a-e** caused redshifts in UV-vis spectra in comparison to compound **4a**. All of these ligands' binding interactions with calf thymus DNA (*ct*-DNA) were investigated using spectrophotometric titrations to determine the general affinity of the derivatives **4a-f** to *ct*-DNA. If the compounds are bound with DNA, it is widely assumed that their UV-Vis characteristic curves will exhibit a shift in maximum absorption wavelength (bathochromic or hypsochromic shift) and absorbance (hypochromic or hyperchromicity) [31,32]. All of these ligands' binding interactions with calf thymus DNA

(*ct*-DNA) were investigated using spectrophotometric titrations to determine the general affinity of the derivatives **4a-f** to *ct*-DNA. If the compounds bounded with *ct*-DNA, it is widely assumed that their UV-Vis characteristic curves will show a shift in maximum absorption wavelength (bathochromic or hypsochromic shift) and absorbance (hypochromicity or hyperchromicity). All the synthesized compounds **4a-f** produced either hyperchromic or hypochromic effects with *ct*-DNA, with compound **4f** producing the most hypochromic effects (Table-3).

After the compound penetrated the DNA base pairs, the orbitals of the penetrated compounds coupled with the orbitals of the base pairs, lowering the transition energies [33]. This penetration caused the above hypochromic, which predicts penetration [34]. Furthermore, the hypochromic effect and redshift of the absorption maximum are features of the ligand's interaction with DNA, as observed with *ct*-DNA and thiazaridine [35]. These findings show that the pyrazole ring is important in the DNA interaction process and that hyperchromic and hypochromic effects, as well as red or blue shifts, reflect varying degrees of DNA helix structure changes [36]. The imino naphthyl pyrazole derivatives' DNA binding constants ( $K_b$ ) were calculated using intensity changes during absorbance (Table-3). The values of  $K_b$ , which range from  $1.74 \times 10^4$  to  $1.0 \times 10^6 M^{-1}$ , indicate that these pyrazole derivatives have a high affinity for *ct*-DNA base pairs. The  $K_b$  values for penetrated complexes between organic dyes and DNA typically range from  $1 \times 10^4$  to  $1 \times 10^6 M^{-1}$  and are smaller than the binding constants of groove binders ( $1 \times 10^5$  to  $1 \times 10^9 M^{-1}$ ). The  $K_b$  values increased in the following order: **4d** < **4e** < **4c** < **4b** < **4a** < **4f**. The high  $K_b$  value of **4f** indicates a strong affinity for *ct*-DNA binding. The nitro-substituted derivative **4f** had the highest  $K_b$  value ( $1.0 \times 10^6$ ), indicating that the nitro substituent positively affects the ligand's binding capacity with *ct*-DNA by increasing the ligand's hydrophobic properties. Furthermore, the presence of a nitro group increases the compound's polarity, increasing dipole-dipole interactions in the binding site and acting as a hydrogen-bond acceptor. Moreover, the consistency of the magnitude of  $K_b$  for different substituted pyrazole terminated imino naphthyl derivatives supports the hypothesis that the binding mechanism with DNA is primarily dependent on a common structural feature of all studied compounds, namely diphenyl substituted pyrazole imino naphthyl. However, its lateral substituents influence binding to a lesser extent [33].

Table-3 summarizes the results of spectrofluorimetric studies conducted to investigate the binding properties of

pyrazole imino naphthyl derivatives and *ct*-DNA. Compounds **4a-f** exhibited an emission band in the 400-500 nm range, with excitation wavelengths in the 350-370 nm range and spectra were scanned at a fixed concentration of 15  $\mu M$  of each derivative and various *ct*-DNA concentrations (Fig. 3). The addition of *ct*-DNA quenched the fluorescence of pyrazole derivatives, except for compounds **4b** and **4c** derivatives, which showed an increase in fluorescence intensity as the concentration of DNA was increased. In general, the magnification of fluorescence intensity can be denoted by a significant quenching of the ligand's conformational flexibility within the DNA-ligand complex. Fig. 4 depicts the emission spectra of **4a** in the presence of various concentrations of *ct*-DNA.

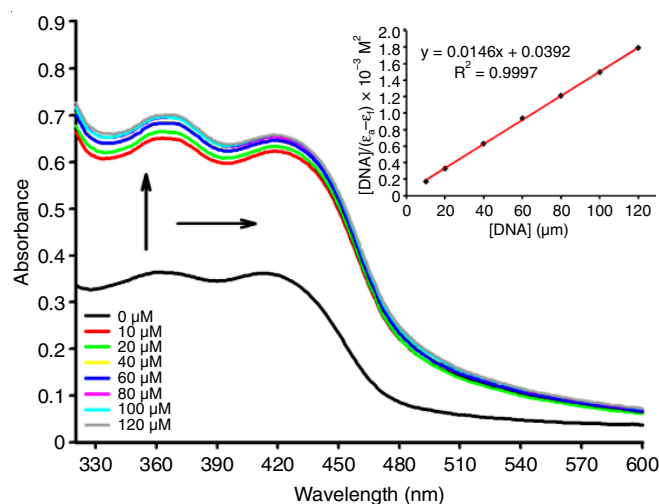


Fig. 3. Absorption spectra of derivative **4b** (50  $\mu M$ ) with increasing concentrations of *ct*-DNA. [DNA] = 0, 10, 20, 40, 60, 80, 100 and 120  $\mu M$ . Arrows ( $\uparrow$ ) and ( $\rightarrow$ ) refer to hyperchromic and bathochromic effects, respectively. Inset: Plot of  $[DNA]/(\epsilon_0 - \epsilon_r)$  as a function of DNA concentration as determined from the absorption spectral data

A plot of the relative emission intensity,  $I_0/I$ , vs. the concentration of DNA was made to estimate the efficiency of quenching process (Fig. 5). When the Stern-Volmer constant ( $K_{SV}$ ) for quenching was computed, marked quenching was revealed by the **3f** derivative ( $2.18 \times 10^4 M^{-1}$ ), with the order **4f** > **4a** > **4d** > **4c** > **4e** > **4b**. The electron transfer between the *ct*-DNA bases and the excited ligand was most likely responsible for the reduction in emission intensity caused by the addition of DNA. The synthesized compounds' Stern-Volmer ( $K_{SV}$ ) and binding constants ( $K_b$ ) indicated static quenching due to the interaction and thus forming a complex with *ct*-DNA. The

TABLE-3  
UV-VIS ABSORPTION AND FLUORESCENCE EMISSION DATA OF NEW ACRIDINE-THIOSEMICARBAZONE DERIVATIVES IN THE ABSENCE AND PRESENCE OF *ct*-DNA

Compd.	$\lambda_{max}$ (nm)		Extinction coefficient $\epsilon$ ( $M^{-1}$ )	$\Delta\lambda$ (nm)	Hypochr. (%) <sup>a</sup>	Hyperchr. (%) <sup>b</sup>	$K_b \times 10^5$ ( $M^{-1}$ )	$\lambda_{exit}$ (nm)	$\Lambda_{emis}$ (nm)	$K_{SV} \times 10^4$ ( $M^{-1}$ )
	Absent	Present								
<b>4a</b>	360	366	7.300	6	–	92.58	3.77	359	439	0.92
<b>4b</b>	375	372	8.600	3	–	28.14	1.84	370	441	-0.20
<b>4c</b>	376	375	13.780	1	20.32	–	1.20	370	440	0.18
<b>4d</b>	375	372	14.041	4	4.69	–	1.74	370	441	0.87
<b>4e</b>	375	372	8.760	4	–	25.22	6.50	361	441	-0.27
<b>4f</b>	362	362	9.200	0	–	24.4	9.91	352	439	0.50

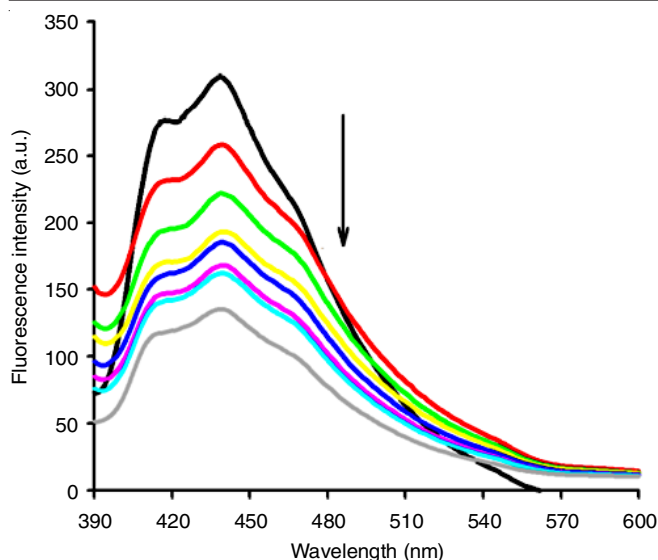


Fig. 4. Fluorescence spectra of derivative **4a** (15  $\mu\text{M}$ ) with increasing concentrations of *ct*-DNA. [DNA] = 0 (black), 10 (red), 20 (green), 40 (yellow), 60 (blue), 80 (pink), 100 (light blue) and 120 (gray)  $\mu\text{M}$ . Arrow ( $\downarrow$ ) refers to hypochromic effect

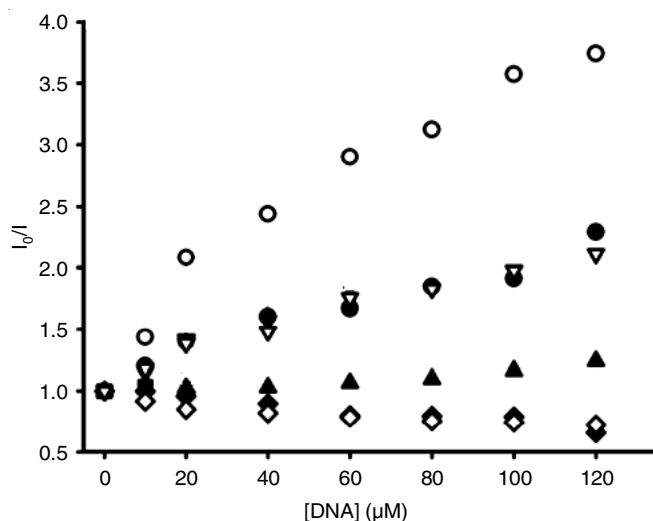


Fig. 5. Relative fluorescence intensities of pyrazole derivatives **4a** (●), **4b** (◇), **4c** (▲), **4d** (△), **4e** (◆) and **4f** (○), upon addition of *ct*-DNA in Tris buffer (0.01 M, pH = 7.6)

analysis revealed that the compound **4f** was the most efficient at bonding to *ct*-DNA *in vitro* (39.59% hypochromic effect and the highest  $K_b$ ,  $K_{SV}$  values). Fluorescence emission studies shed light on the interaction of *ct*-DNA, with increasing amounts of *ct*-DNA resulting in a decrease in fluorescence intensity without a significant shift in maximum fluorescence emission wavelength, indicating *ct*-DNA binding. Because both the “light up” and “light off” effects were detected in fluorescence emission spectra, the new pyrazole terminated imino naphthyl derivatives could interact with *ct*-DNA in this study.

**DNA molecular docking:** Molecular docking analysis is an appealing tool for recognizing the nature of drug–DNA interaction for drug planning, synthesis, design and development as a new chemotherapeutic compound, as well as studying its mechanism when a new molecule is introduced into the binding site of the DNA target specific region of the DNA, primarily in a non-covalent manner. Even though different

properties exist, we concentrated on the structure of compound to regulate binding modes such as a major or minor groove within the DNA. Several forces, including weak van der Waals forces, hydrogen bonding, hydrophobicity, charge transfer and electrostatic complementarity, have been shown in the literature to stabilize DNA–intercalator complexes [37,38]. Molecular docking with DNA aids in understanding the firmness of the compound’s suitable confirmation within the binding location of DNA to act as a biologically active drug. Docking of the synthesized pyrazole derivatives (**4a–f**) with *ct*-DNA duplex of the sequence d(CGCGAATTCGCG)2 dodecamer (PDB ID: 355D) was performed in AutoDock 4.1 module to predict the preferred orientation of the compounds inside the DNA helix and the most favourable docked poses are shown in Fig. 6. since all the synthesized compounds have a similar structure, they can interact with DNA near the minor groove and the planarity of the compounds strengthens the binding of these compounds *via* partial intercalation with DNA. According to the literature, smaller molecules prefer to interact with minor groove of the DNA due to less steric hindrance [39]. Furthermore, an aromatic ring connected by a single bond allows for a torsional strain to facilitate groove curvature with the elimination of water molecules. Furthermore, the molecule’s heterocyclic moiety promotes stacking interactions between DNA base pairs, resulting in van der Waals and hydrophobic contacts with DNA functional groups that define the groove [26].

## Conclusion

Six new 1-phenyl-3-nitrophenyl pyrazole linked imino naphthyl derivatives were synthesized, characterized and tested *in vitro* against Gram-negative bacterial strains such as *E. coli* MTCC-443 and *Pseudomonas aeruginosa* MTCC-1688 and two Gram-positive strains as *Staphylococcus aureus* MTCC-96 and *Streptococcus pyogenes* MTCC-442. Its antifungal and antituberculosis properties were also investigated. The biological activities of synthesized compounds could be attributed to the greater lipophilicity of two different phenyls and one naphthyl group attached to the pyrazole entity. Furthermore, the electron-withdrawing substituent present in the fourth position of the imino naphthyl ring increased its biological activity. Computational molecular docking studies assisted in determining the minimum ligand pose binding energy and H-bond length of all compounds synthesized in the target protein TMPK. The pyrazole terminated imino naphthyl derivatives (**4a–f**) demonstrated binding constants with *ct*-DNA ranging from  $1.74 \times 10^4$  to  $1.0 \times 10^6 \text{ M}^{-1}$  and quenching constants ranging from  $0.2 \times 10^4$  to  $2.18 \times 10^4 \text{ M}^{-1}$ , indicating high affinity to *ct*-DNA base pairs. Most of the compounds exhibited a combination of hyperchromic or hypochromic effects as well as red or blue shifts. Similarly, molecular docking with DNA results in non-covalent interactions that enter the minor groove binding mode.

## ACKNOWLEDGEMENTS

The authors thank STIC, Cochin University of Science and Technology, for providing  $^1\text{H}$  and  $^{13}\text{C}$  NMR, FTIR and UV-Vis data. Thanks are also due to Department of Chemistry, IIT Chennai for providing computational facilities (docking) and Advanced Molecular Materials Research Centre, Mahatma

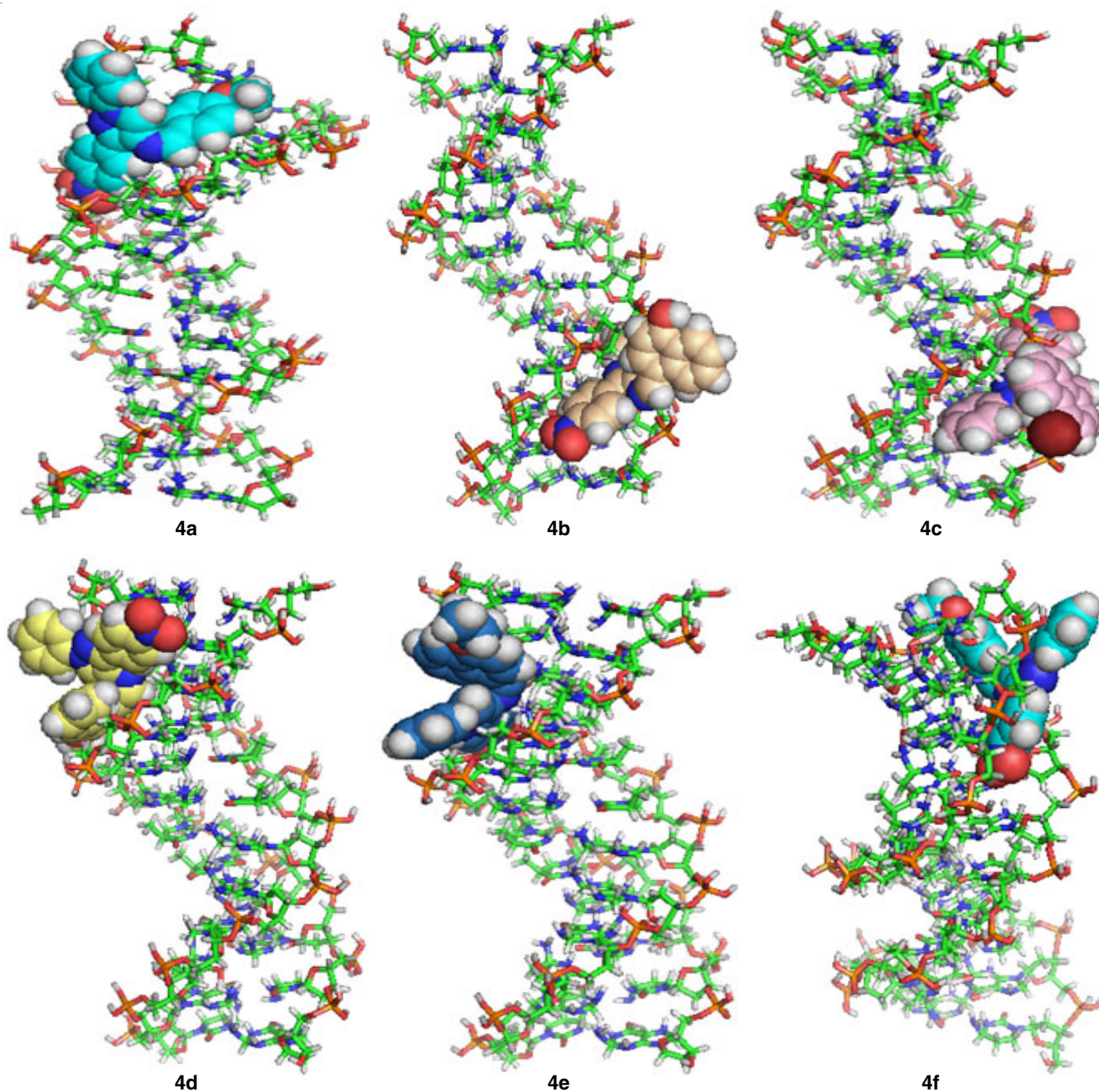


Fig. 6. Molecular docked model of **4a-4f** with DNA dodecamer duplex of sequenced (CGCGAATTCGCG)<sub>2</sub> (PDB ID: 1BNA)

Gandhi University, Kottayam, India for providing fluorescence spectra.

## REFERENCES

1. A.M. Vijesh, A.M. Isloor, P. Shetty, S. Sundershan and H.K. Fun, New Pyrazole Derivatives containing 1,2,4-triazoles and Benzoxazoles as Potent Antimicrobial and Analgesic Agents, *Eur. J. Med. Chem.*, **62**, 410 (2013); <https://doi.org/10.1016/j.ejmech.2012.12.057>
2. W. Akhtar, A. Marella, M.M. Alam, M.F. Khan, M. Akhtar, T. Anwer, F. Khan, M. Naematullah, F. Azam, M.A. Rizvi and M. Shaquiquzzaman, Design and Synthesis of Pyrazole-Pyrazoline Hybrids as Cancer-Associated Selective COX-2 Inhibitors, *Arch. Pharm.*, **354**, 2000116 (2021); <https://doi.org/10.1002/ardp.202000116>
3. M.D. Carrión, L.C. López Cara, M.E. Camacho, V. Tapias, G. Escames, D. Acuña-Castroviejo, A. Espinosa, M.A. Gallo and A. Entrena, Pyrazoles and Pyrazolines as Neural and Inducible Nitric Oxide Synthase (nNOS and iNOS) Potential Inhibitors (III), *Eur. J. Med. Chem.*, **43**, 2579 (2008); <https://doi.org/10.1016/j.ejmech.2008.01.014>
4. N. Gökhan-Kelekçi, S. Koyunoglu, S. Yabanoglu, K. Yelekçi, Ö. Özgen, G. Uçar, K. Erol, E. Kendi and A. Yesilada, New Pyrazoline Bearing 4(3H)-Quinazolinone Inhibitors of Monoamine Oxidase: Synthesis, Biological Evaluation and Structural Determinants of MAO-A and MAO-B Selectivity, *Bioorg. Med. Chem.*, **17**, 675 (2009); <https://doi.org/10.1016/j.bmc.2008.11.068>
5. J.V. Faria, P.F. Vegi, A.G.C. Miguita, M.S. dos Santos, N. Boechat and A.M.R. Bernardino, Recently Reported Biological Activities of Pyrazole Compounds, *Bioorg. Med. Chem.*, **25**, 5891 (2017); <https://doi.org/10.1016/j.bmc.2017.09.035>
6. M. Abid, A.R. Bhat, F. Athar and A. Azam, Synthesis, Spectral Studies and Antiamoebic Activity of New 1-N-Substituted Thiocarbonyl-3-phenyl-2-pyrazolines, *Eur. J. Med. Chem.*, **44**, 417 (2009); <https://doi.org/10.1016/j.ejmech.2007.10.032>

7. A.M. Farag, A.S. Mayhoub, S.E. Barakat and A.H. Bayomi, Synthesis of New N-Phenylpyrazole Derivatives with Potent Antimicrobial Activity, *Bioorg. Med. Chem.*, **16**, 4569 (2008); <https://doi.org/10.1016/j.bmc.2008.02.043>
8. S.R. Shih, T.-Y. Chu, G.R. Reddy, S.-N. Tseng, H.-L. Chen, W.-F. Tang, M. Wu, J.-Y. Yeh, Y.-S. Chao, J.T.A. Hsu, H.-P. Hsieh and J.-T. Horng, Pyrazole Compound BPR1P0034 with Potent and Selective Anti-Influenza Virus Activity, *J. Biomed. Sci.*, **17**, 13 (2010); <https://doi.org/10.1186/1423-0127-17-13>
9. H. Naito, S. Ohsuki, M. Sugimori, R. Atsumi, M. Minami, Y. Nakamura, M. Ishii, K. Hirotsu, E. Kumazawa and A. Ejima, Synthesis and Antitumor Activity of Novel Pyrimidinyl Pyrazole Derivatives. II. Optimization of the Phenylpiperazine Moiety of 1-[5-Methyl-1-(2-pyrimidinyl)-4-pyrazolyl]-3-phenylpiperazinyl-1-*trans*-propenes, *Chem. Pharm. Bull. (Tokyo)*, **50**, 453 (2002); <https://doi.org/10.1248/cpb.50.453>
10. M. Abdel-Aziz, G.E.D.A. Abu-Rahma and A.A. Hassan, Synthesis of Novel Pyrazole Derivatives and Evaluation of their Antidepressant and Anticonvulsant Activities, *Eur. J. Med. Chem.*, **44**, 3480 (2009); <https://doi.org/10.1016/j.ejmech.2009.01.032>
11. A.M. Farag, A.S. Mayhoub, S.E. Barakat and A.H. Bayomi, Regioselective Synthesis and Antitumor Screening of Some Novel N-phenylpyrazole Derivatives, *Bioorg. Med. Chem.*, **16**, 881 (2008); <https://doi.org/10.1016/j.bmc.2007.10.015>
12. K. Karrouchi, S. Radi, Y. Ramli, J. Taoufik, Y. Mabkhot, F. Al-aizari and M. Ansar, Synthesis and Pharmacological Activities of Pyrazole Derivatives: A Review, *Molecules*, **23**, 134 (2018); <https://doi.org/10.3390/molecules23010134>
13. Kavaya, R. Upadhyaya, S. Laxmi and R. Venkateswaran, Effect of Intravenous Dexmedetomidine Administered as Bolus or as Bolus-Plus-Infusion on Subarachnoid Anesthesia with Hyperbaric Bupivacaine, *J. Anaesthesiol. Clin. Pharmacol.*, **34**, 46 (2018); [https://doi.org/10.4103/joacp.JOACP\\_132\\_16](https://doi.org/10.4103/joacp.JOACP_132_16)
14. V. Michon, C.H. du Penhoat, F. Tombret, J.M. Gillardin, F. Lepage and L. Berthon, Preparation, Structural Analysis and Anticonvulsant Activity of 3- and 5-aminopyrazole *N*-Benzoyl Derivatives, *Eur. J. Med. Chem.*, **30**, 147 (1995); [https://doi.org/10.1016/0223-5234\(96\)88220-1](https://doi.org/10.1016/0223-5234(96)88220-1)
15. M. Assali, M. Abualhasan, H. Sawaftah, M. Hawash and A. Mousa, Synthesis, Biological Activity, and Molecular Modeling Studies of Pyrazole and Triazole Derivatives as Selective COX-2 Inhibitors, *J. Chem.*, **2020**, 6393428 (2020); <https://doi.org/10.1155/2020/6393428>
16. N.K. Terrett, A.S. Bell, D. Brown and P. Ellis, Sildenafil (VIAGRA™), A Potent and Selective Inhibitor of Type 5 cGMP Phosphodiesterase with Utility for the Treatment of Male Erectile Dysfunction, *Bioorg. Med. Chem. Lett.*, **6**, 1819 (1996); [https://doi.org/10.1016/0960-894X\(96\)00323-X](https://doi.org/10.1016/0960-894X(96)00323-X)
17. K.R.A. Abdellatif, M.T. Elsaady, N.H. Amin and A.A. Hefny, Design, Synthesis and Biological Evaluation of Some Novel Indole Derivatives as Selective COX-2 Inhibitors, *J. Appl. Pharm. Sci.*, **7**, 069 (2017); <https://doi.org/10.7324/JAPS.2017.70810>
18. J.E. Ancel, L. El Kaïm, A. Gadrás, L. Grimaud and N.K. Jana, Studies Towards the Synthesis of Fipronil® Analogues: Improved Decarboxylation of  $\alpha$ -hydrazonoacid Derivatives, *Tetrahedron Lett.*, **43**, 8319 (2002); [https://doi.org/10.1016/S0040-4039\(02\)01977-9](https://doi.org/10.1016/S0040-4039(02)01977-9)
19. M.J. Alam, O. Alam, P. Alam and M.J. Naim, A Review on Pyrazole Chemical Entity and Biological Activity, *Int. J. Pharm. Sci. Res.*, **6**, 1433 (2015).
20. M. Maaloum, P. Muller and S. Harlepp, DNA-Intercalator Interactions: Structural and Physical Analysis using Atomic Force Microscopy in Solution, *Soft Matter*, **9**, 11233 (2013); <https://doi.org/10.1039/c3sm52082j>
21. A. Rescifina, C. Zagni, M.G. Varrica, V. Pistorà and A. Corsaro, Recent Advances in Small Organic Molecules as DNA Intercalating Agents: Synthesis, Activity and Modeling, *Eur. J. Med. Chem.*, **74**, 95 (2014); <https://doi.org/10.1016/j.ejmech.2013.11.029>
22. H.E.D. Aboul-Anean, Using Quinoa Protein and Starch Nanoparticles to Produce Edible Natural Films, *J. Nutr. Heal. Food Eng.*, **8**, 297 (2018); <https://doi.org/10.15406/jnhfe.2018.08.00286>
23. A. Balbi, M. Anzaldi, M. Mazzei, M. Miele, M. Bertolotto, L. Ottonello and F. Dallegri, Synthesis and Biological Evaluation of Novel Heterocyclic Ionone-like Derivatives as Anti-inflammatory Agents, *Bioorg. Med. Chem.*, **14**, 5152 (2006); <https://doi.org/10.1016/j.bmc.2006.04.007>
24. A. Pai, D.V. Kumar and B.S. Jayashree, Synthesis, Characterization, Antibacterial and Anticancer Evaluation of Some Novel Flavone-3-ols, *Asian J. Pharm. Sci.*, **11**, 187 (2016); <https://doi.org/10.1016/j.ajps.2015.11.044>
25. N.C. Desai, A. Dodiya and N. Shihory, Synthesis and Antimicrobial Activity of Novel Quinazolinone–Thiazolidine–Quinoline Compounds, *J. Saudi Chem. Soc.*, **17**, 259 (2013); <https://doi.org/10.1016/j.jscs.2011.04.001>
26. M. Baginski, F. Fogolari and J.M. Briggs, Electrostatic and Non-electrostatic Contributions to the Binding Free Energies of Anthracycline Antibiotics to DNA, *J. Mol. Biol.*, **274**, 253 (1997); <https://doi.org/10.1006/jmbi.1997.1399>
27. S. Instruments, Instrumentation for Fluorescence Spectroscopy 2.1, pp. 27-61, Ed. 3 (2000).
28. A.S. Khalil and J.J. Collins, Synthetic Biology: Applications Come of Age, *Nat. Rev. Genet.*, **11**, 367 (2010); <https://doi.org/10.1038/nrg2775>
29. S. Mert, R. Kasimogullari and S. Ok, A Short Review on Pyrazole Derivatives and their Applications, *J. Postdr. Res.*, **2**, 64 (2014).
30. D. Ravi, S. Sarkar, S. Purvey, F. Passero, A. Beheshti, Y. Chen, M. Mokhtar, K. David, T. Konry and A.M. Evens, Interaction Kinetics with Transcriptomic and Secretory Responses of CD19-CAR Natural Killer-Cell Therapy in CD20 Resistant Non-Hodgkin Lymphoma, *Leukemia*, **34**, 1291 (2020); <https://doi.org/10.1038/s41375-019-0663-x>
31. S.F. Baranovsky, P.A. Bolotin, M.P. Evstigneev and D.N. Chernyshev, Interaction of Ethidium Bromide and Caffeine With DNA in Aqueous Solution, *J. Appl. Spectrosc.*, **76**, 132 (2009); <https://doi.org/10.1007/s10812-009-9139-5>
32. E.A. Lafayette, S. Vitalino de Almeida, M. da Rocha Pitta, E. Carneiro Beltrão, T. Gonçalves da Silva, R. Olímpio de Moura, I. da Rocha Pitta, L. de Carvalho and M. do Carmo Alves de Lima, *Molecules*, **18**, 15035 (2013); <https://doi.org/10.3390/molecules181215035>
33. S.M.V. De Almeida, E. Lafayette, L. da Silva, C. Amorim, T. de Oliveira, A. Ruiz, J. de Carvalho, R. de Moura, E. Beltrão, M. de Lima and L. Júnior, Synthesis, DNA Binding, and Antiproliferative Activity of Novel Acridine-Thiosemicarbazone Derivatives, *Int. J. Mol. Sci.*, **16**, 13023 (2015); <https://doi.org/10.3390/ijms160613023>
34. A. Chilin, G. Marzaro, C. Marzano, L.D. Via, M.G. Ferlin, G. Pastorini and A. Guiotto, Synthesis and Antitumor Activity of Novel Amsacrine Analogs: The Critical Role of the Acridine Moiety in Determining their Biological Activity, *Bioorg. Med. Chem.*, **17**, 523 (2009); <https://doi.org/10.1016/j.bmc.2008.11.072>
35. A.K. Das, H. Ihmels and S. Kölsch, Diphenylaminostyryl-Substituted Quinolizinium Derivatives as Fluorescent Light-up Probes for Duplex And Quadruplex DNA, *Photochem. Photobiol. Sci.*, **18**, 1373 (2019); <https://doi.org/10.1039/C9PP00096H>
36. J. Kah, C. Yong and Z. Xu, New Developments in Gold Nanomaterials Research, Nova Science Publishers Inc. U.K., Ed. 1 (2016).
37. I. Sultan, S. Rahman, A.T. Jan, M.T. Siddiqui, A.H. Mondal and Q.M.R. Haq, Antibiotics, Resistome and Resistance Mechanisms: A Bacterial Perspective, *Front. Microbiol.*, **9**, 2066 (2018); <https://doi.org/10.3389/fmicb.2018.02066>
38. S. Tomassi, J. Lategahn, J. Engel, M. Keul, H.L. Tumbrink, J. Ketzer, T. Mühlenberg, M. Baumann, C. Schultz-Fademrecht, S. Bauer and D. Rauh, Indazole-Based Covalent Inhibitors to Target Drug-Resistant Epidermal Growth Factor Receptor, *J. Med. Chem.*, **60**, 2361 (2017); <https://doi.org/10.1021/acs.jmedchem.6b01626>
39. R. Røhs, I. Bloch, H. Sklenar and Z. Shakked, Molecular Flexibility in *ab initio* Drug Docking to DNA: Binding-Site and Binding-Mode Transitions in All-Atom Monte Carlo Simulations, *Nucleic Acids Res.*, **33**, 7048 (2005); <https://doi.org/10.1093/nar/gki1008>